

# Asymmetric parametric generation of images with nonlinear dielectric metasurfaces

Sergey S. Kruk<sup>1,2#\*</sup>, Lei Wang<sup>2, 3#\*</sup>, Basudeb Sain<sup>1</sup>, Zhaogang Dong<sup>4</sup>, Joel Yang<sup>4,5</sup>,  
Thomas Zentgraf<sup>1</sup>, and Yuri Kivshar<sup>2\*</sup>

<sup>1</sup>Department of Physics, Paderborn University, 33098 Paderborn, Germany

<sup>2</sup>Nonlinear Physics Center, Research School of Physics, Australian National University,  
Canberra ACT 2601, Australia

<sup>3</sup>National Mobile Communications Research Laboratory, Quantum Information Center, Southeast  
University, Nanjing 210096, China

<sup>4</sup>Institute of Materials Research and Engineering, A\*STAR (Agency for Science Technology,  
and Research), Singapore 138634, Singapore

<sup>5</sup>Singapore University of Technology and Design, Singapore 487372, Singapore

#These authors contributed equally to this work

\*E-mails: sergey.kruk@outlook.com, wang\_lei\_seu@seu.edu.cn, ysk@internode.on.net

## **Abstract**

Subwavelength dielectric resonators assembled into metasurfaces have become versatile tools to miniaturise optical components towards the nanoscale. An important class of such functionalities is associated with asymmetries in both generation and propagation of light with respect to reversals of the positions of transmitters and receivers. A promising pathway towards miniaturisation of asymmetric light control is via *nonlinear light-matter interactions*. Here we demonstrate asymmetric parametric generation of light at the level of individual subwavelength resonators. We assemble thousands of dissimilar nonlinear dielectric resonators into translucent metasurfaces that produce images in the visible spectral range when illuminated by infrared radiation. By design, these nonlinear metasurfaces produce different and completely independent images for the reversed directions of illumination, that is when the positions of the infrared transmitter and the visible light receiver are exchanged. Nonlinearity-enabled asymmetric control of light at the level of individual subwavelength resonators opens an untapped potential for developing novel nanophotonic components via dense integration of large quantities of nonlinear resonators into compact metasurfaces.

## Introduction

Optical materials undergo revolutionary transformations driven by nanotechnology. Our ability to engineer optical structures at a scale smaller than the wavelength of light enables new properties and functionalities not available in unstructured bulk materials. A class of recently emerged nano-optics components – *dielectric metasurfaces* – employs two-dimensional arrays of designer resonant nanoscale elements whose optical response is defined by their geometry [1–3].

While linear regimes of interactions between dielectric metasurfaces and moderately intense light have already formed a vast landscape of applied research and engineering, new frontiers are being actively explored in the nonlinear optical regime describing interactions of metasurfaces with strong optical fields [4–6]. Recently, significant progress has been made in increasing the efficiency of nonlinear processes in subwavelength nanophotonics facilitated by designs utilizing high index dielectric nanoparticles supporting multipolar Mie resonances [7–10] and composite modes [11–13].

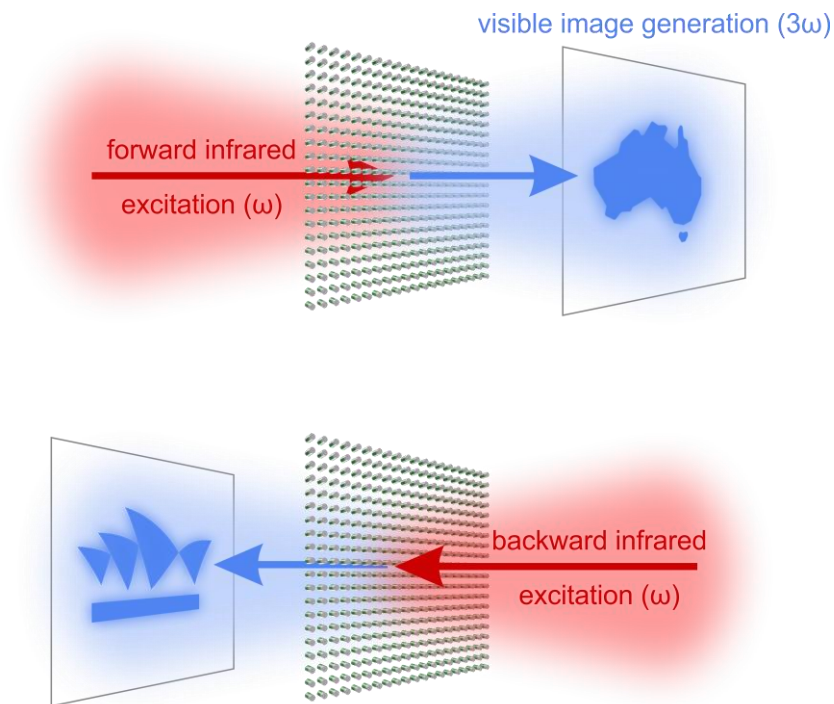


**Figure 1. Concept of asymmetric parametric generation of images with nonlinear metasurface.** The metasurface generates different and independent images in transmission for two opposite illumination directions. The images are produced at tripled frequency via a nonlinear process of third-harmonic generation.

Nonlinearities render basic principles of interactions between light and matter, such as superposition principle, geometric optics approximation, and optical reciprocity. This allows to acquire novel functionalities of metasurfaces beyond those of their linear counterparts. Recent examples include imaging through nonlinear meta-lenses governed by a generalized lens equation [14], spatial correlations of light [15], nonlinear topological transitions [16], bistability [17], and optical pulse shaping [18] among others.

An important cluster of functionalities enabled by nonlinear light-matter interactions is associated with asymmetric control of light, which resembles some similarities with asymmetric control of electrical currents with nanoscale semiconductor diodes. Traditionally, such functionalities are associated with bulky optical

components [19–21]. Relatively more compact photonic chips with coupled waveguide resonators [22] were demonstrated to enable asymmetric control of light. Recently, there has been an interest in theoretical investigations of various nonlinear nanophotonics platforms for asymmetric light control [23–27]. A plasmonic metasurface with asymmetries in nonlinear light generation was demonstrated experimentally [28].

However, the approaches demonstrated to date rely on optical components that are substantially larger than the wavelength of light in at least two spatial dimensions, including demonstrated systems of optical waveguides [22] and phase gradient metasurfaces [28]. This hinders dense integration of large quantities of such photonic components into compact systems analogous to integration of large quantities of electronic components into semiconductor chips.

Here we design and demonstrate all-dielectric metasurfaces with nonlinear asymmetric generation of light at a level of individual nanoresonators. We assemble approximately 15 000 nanoresonators of varying design into metasurfaces with a footprint of approximately  $0.012 \text{ mm}^2$ . When infrared light passes through the metasurfaces, certain encoded images are observed, as sketched in the Fig. 1. However, once we flip the metasurfaces to the opposite side, we observe completely different images. This is achieved by judiciously designing a set of constituent nanoresonators each performing its own operation by generating either high or low intensity of light depending on the direction of illumination (from the front or from the back). This effect is underpinned by a novel regime of nonlinear interaction between electric and magnetic modes rendered by magneto-electric coupling.

The functionality of the developed resonators relies on an interplay between nonlinear light-matter interactions and magneto-electric coupling [29] to its artificially engineered optical modes. Upon such coupling, the magnetic-type optical resonances are induced by both electric and magnetic components of an incident light beam. Magneto-electric coupling has facilitated many peculiar photonic functionalities both in microwaves and optics, including polarisation transformations [30,31], anomalous transmission [32,33] and reflection [34,35]; photonic analogues of spin-Hall effects [36], photonic Jackiw-Rebbi states [37], and nontrivial topological phases [38].

### **Identical asymmetric nonlinear resonators**

We employ metasurfaces made of dielectric nano-cylinders. We design the nanoresonators such that their optical response at the fundamental wavelength is dominated by two Mie multipoles: electric and magnetic dipole modes with smaller contributions from higher-order multipoles [39] [40]. Furthermore, our resonators consist of two layers of materials with different optical constants: amorphous silicon and silicon nitride [see Figs. 2a,b]. Silicon in comparison to silicon nitride has a higher refractive index and higher nonlinear susceptibility. Geometrically, our resonator is symmetric, and magneto-electric coupling rises purely from the refractive index distribution within the cylinder. This symmetrical design of the bilayer nanoresonator is of particular interest for nanophotonics as it is suitable for fabrication with standard nanotechnologies.

We proceed with full-wave numerical simulations. Figures 2a,b show a particular example of a bi-layer nanoresonator forming a uniform metasurface with all the geometrical parameters listed in the figure captions (see Supporting Information for our optimization approach of the geometrical parameters). We start from the simplest case of a metasurface embedded into a homogeneous environment (glass). In this setting, the only asymmetry the metasurface possesses with respect to “forward” and “backward” directions comes solely from the bi-layer silicon/silicon nitride design. We calculate linear scattering of the nanoresonators within the metasurface (see details in Methods). They feature identical total scattering with respect to “forward” and “backward” illumination as required by reciprocity (black curves in Figs. 2c,d). However, the anisotropy of the resonators’ design reveals itself in a decomposition of the total scattering into a series of Mie multipoles that is drastically different. While the “forward” illumination leads to predominantly magnetic dipole-type

scattering, for the “backward” illumination the scattering is dominated by an electric dipole (see orange solid and purple dashed curves in Figs. 2c,d). Remarkably, in the forward (backward) direction, the electric (magnetic) dipoles are almost completely suppressed at around 1475 nm wavelength.

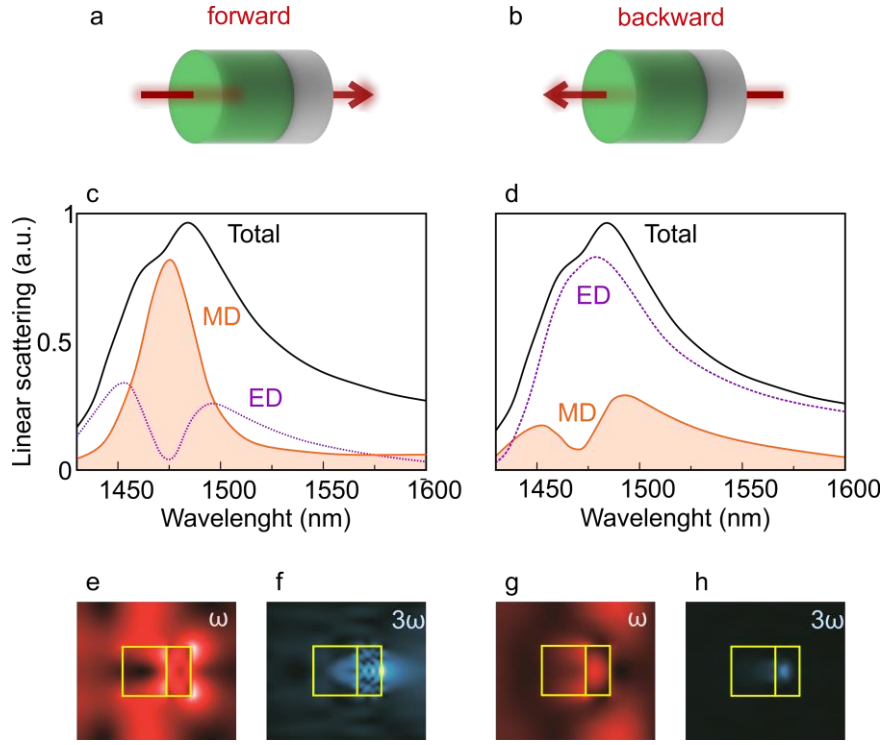


**Figure 2. Optical properties of an individual metasurface element.** (a,b) An anisotropic cylindrical nanoresonator 430 nm in diameter consisting of two materials: silicon (grey) 220 nm thick and silicon nitride (green) 400 nm thick embedded into glass. The nanoresonators are arranged into a square lattice with 925 nm period forming a metasurface. Arrows visualise forward (a) and backward (b) directions of excitation. (c,d) Linear scattering spectra of the nanoresonator in the lattice for forward (c) and backward (d) excitations. (e,g) Near-field distributions of the electric field amplitude at an excitation wavelength of 1475 nm for (e) forward and (g) backward directions. (f,h) Near-field distributions the electric field amplitude of third-harmonic wavelength of ~492 nm for forward (f) and backward (h) excitations at 1475 nm wavelength. Yellow lines mark contours of the bilayer nanoresonator.

To yield a simplistic analytical insight, we approximate the optical response of our nanoresonators down to only electric and magnetic dipole modes leaving weaker higher-order multipoles without consideration. We assume that the metasurface response can be grasped by effective polarizability tensors  $\bar{\alpha}_{ee}$  (electric),  $\bar{\alpha}_{mm}$  (magnetic), and  $\bar{\alpha}_{me}$  (magnetolectric). Without lack of generality, we will focus on x-polarized light beams propagating in  $\pm z$  directions. The response will thus be governed by  $\alpha_{ee}^{xx}$ ,  $\alpha_{mm}^{yy}$ ,  $\alpha_{me}^{xy}$ , and  $\alpha_{me}^{yx}$  components of the tensors. We further assume that the metasurface obeys optical reciprocity in the linear regime. We also take into account that the metasurfaces are engineered from common amorphous dielectrics. This further reduces the number of polarizability terms:  $\alpha_{me}^{xy} = -\alpha_{me}^{yx}$ . Under this condition, the excitation of the electric and the magnetic dipole modes can be written as:

$$\begin{aligned} p_x &= \alpha_{ee}^{xx} E_x \pm \alpha_{me}^{xy} H_y \\ m_y &= \pm \alpha_{mm}^{yy} H_y - \alpha_{me}^{xy} E_x \end{aligned} \quad (1)$$

where  $E_x$  and  $H_y$  are local fields at the position of a nanoresonator. The “ $\pm$ ” sign in front of the “ $H_y$ ” terms accounts for the cases of forward/backward illumination. From Eqs. 1 we can see that the magnetic dipole mode is enhanced for the forward illumination, and it is suppressed for the backward illumination by the magneto-electric coupling. The enhancement/suppression of the electric dipole mode is the opposite to that of the magnetic dipole. Notably, the strength of magneto-electric coupling described by  $\alpha_{me}^{xy}$  conceptually may take arbitrary large values, reaching or even exceeding the strengths of electric and magnetic responses described via  $\alpha_{ee}^{xx}$  and  $\alpha_{mm}^{yy}$  components [41,42]. Interestingly, a balance between the polarizability tensors may lead to complete suppression of a given dipole mode for a given direction of excitation:

$$\begin{aligned} p_x = 0 & \quad \text{for } Z_0 \alpha_{ee}^{xx} = \alpha_{me}^{xy} \quad \text{and forward } (+H_y) \text{ propagation} \\ m_y = 0 & \quad \text{for } \frac{1}{Z_0} \alpha_{mm}^{yy} = \alpha_{me}^{xy} \quad \text{and backward } (-H_y) \text{ propagation} \end{aligned} \quad (2)$$

where  $Z_0$  is the free space impedance.

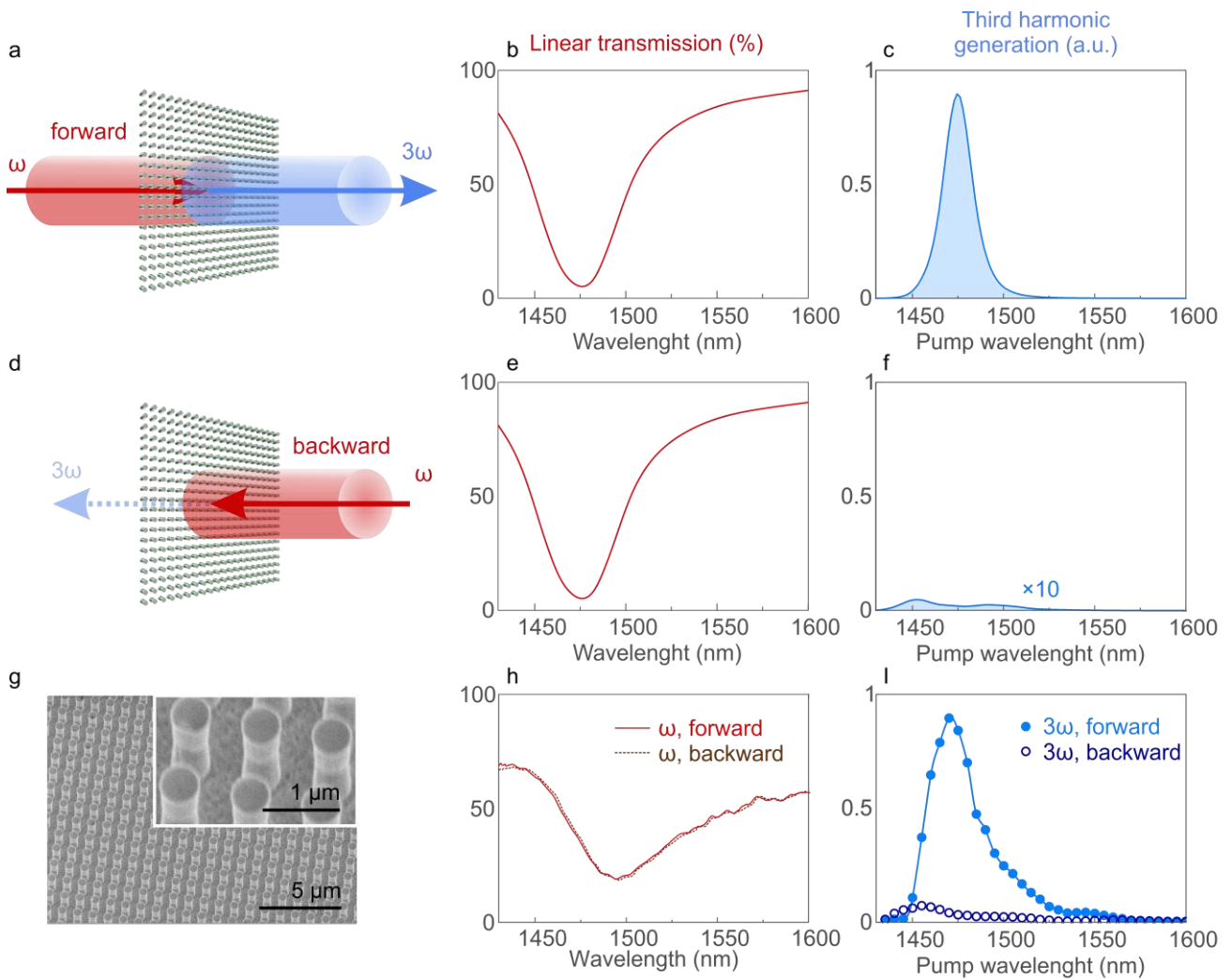


**Figure 3. Symmetric *linear* and asymmetric *nonlinear* spectral response of a uniform metasurface.** (a-f) Theoretical and (g-i) experimental characteristics of a metasurface consisting of identical elements described in Fig. 2. For forward (a) and backward (d) scenarios of excitation the metasurface features identical linear transmission spectra both in theory (b,e) and in experiment (h). However, for the two excitation scenarios, the metasurface demonstrates a drastically different intensity of third harmonic generation both in theory (c,f) and in experiment (i). We note that the third harmonic intensity in (f) is increased 10 times for clearer data representation.

Next, we include into consideration nonlinear light-matter interactions, and we perform full-wave simulations of the generation of third optical harmonics within the nanoresonators under intense laser illumination (see details in Methods). Third harmonic generation (THG) is a process upon which three photons from an excitation beam get “combined” into a single photon with tripled energy and correspondingly tripled frequency. The THG efficiency of a nanoresonator depends on type of an optical mode excited within the resonator, and it is drastically higher for the magnetic dipole-type resonance compared to the electric dipole resonance [28]. As can be seen from Figs. 2e,g, the field enhancements within the nanoresonator are substantially higher for the magnetic dipole-type response (“forward” excitation) than they are for the electric dipole-type response (“backward” direction). This leads to a drastic difference in brightness of the generated third harmonic signal as can be seen in Figs. 2f,h.

We fabricate the metasurface with electron beam lithography (see details in Methods and an image of a fabricated metasurface in Fig. 3g). We perform experimental measurements for both “forward” and “backward” illumination scenarios as illustrated in Figs. 3a,d. We measure linear transmission of the metasurfaces and complement it with numerical simulations (see Figs. 3b,e,h). The linear transmission spectra look identical for “forward” and “backward” scenarios. We next measure the intensity of the third-harmonic signal in the transmission direction for both scenarios of excitation and complement it with numerical simulations (see Figs. 3c,f,i). We observe a striking difference in the intensity of the third harmonic generation.

### **Dissimilar asymmetric nonlinear resonators**

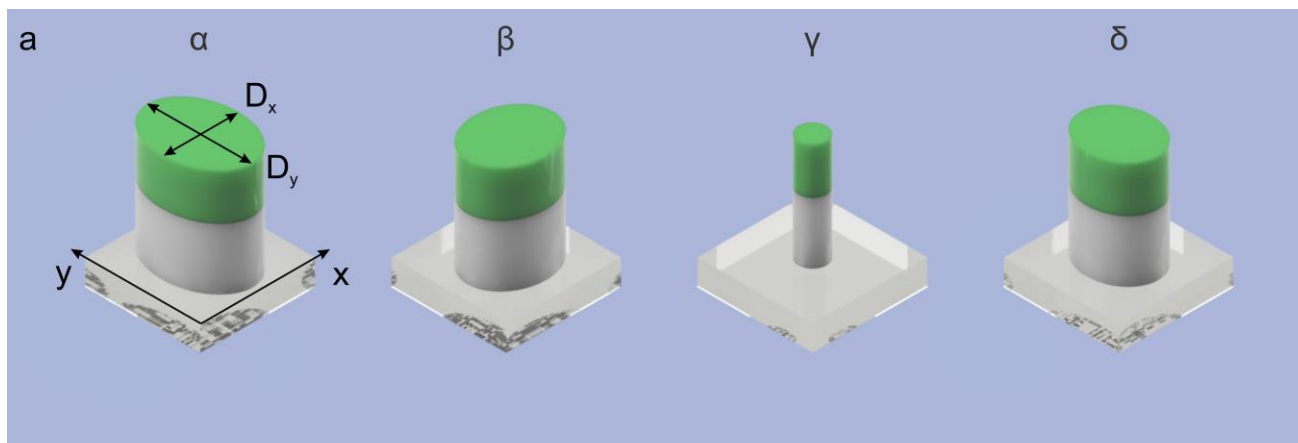
We proceed from uniform metasurfaces consisting of identical nanoresonators to non-uniform metasurfaces assembled from a set of dissimilar resonators. This allows us to develop metasurfaces that generate completely different images for “forward” and “backward” excitations. Here individual nanoresonators serve as “pixels” forming the images.

We limit ourselves to images with binary intensity, e.g., made of dark/bright pixels. A metasurface that produces such binary independent images for the “forward” and “backward” directions would need at least four different types of nanoresonator pixels: an *always bright* pixel, an *always dark* pixel, a pixel that is *bright for the “forward”, but is dark for the “backward”* directions, and finally a pixel with the opposite functionality that is *dark for “forward” but is bright for “backward”*. To design such a set of four pixels, we introduce two additional degrees of freedom to the nanoresonators’ geometry.

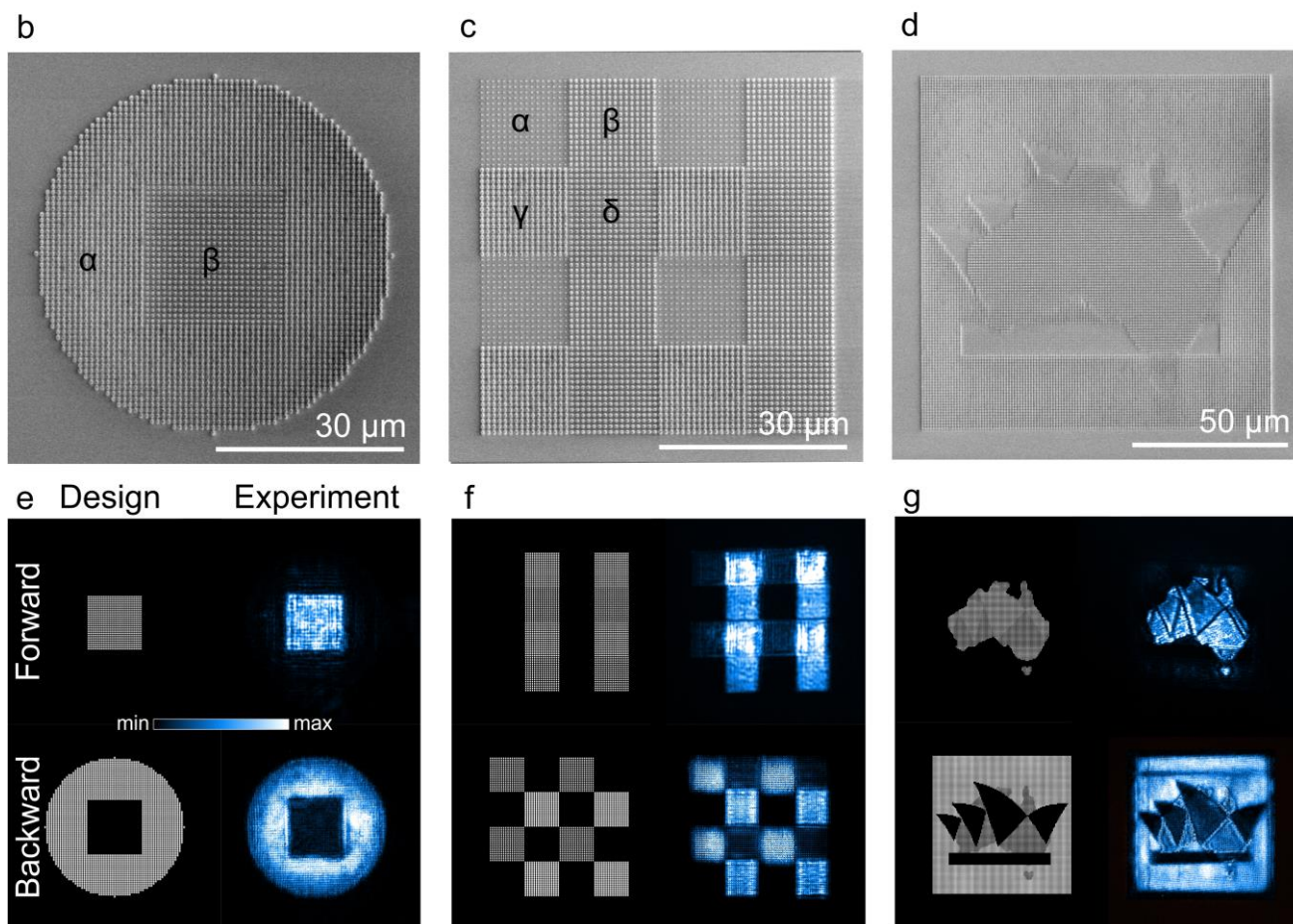
First, we place the resonators on a glass substrate in air. Thus, the resonators are no longer embedded into a homogeneous environment. In this setting, the resonators have two competing sources of asymmetry: the presence of a glass substrate, and the bi-layer design. Second, we allow cylinders with elliptical cross-sections. An extra geometrical parameter (ellipticity of the cross-section) allows us to equalise relative brightness levels of the four resonators. We choose to vary ellipticity and no other geometrical parameter (e.g., thickness of layers) as it adds no extra complexity to the nanofabrication. It is worth noting that ellipticity of resonators may bring additional polarization effects, therefore all our studies we perform for a fixed polarization for all scenarios. The polarization is also parallel to one of the ellipse axes for all resonators so the nanoresonators do not introduce polarisation conversion or any other additional effects.

Figure 4a shows the four designed resonators marked  $\alpha$ ,  $\beta$ ,  $\gamma$ ,  $\delta$  and their corresponding nonlinear optical responses to the “forward” and “backward” directions of excitation. All the resonators have an identical thickness of layers, and the same unit cell size listed in the figure caption. Parameters of the elliptical cross-sections of each resonator type as specified in Fig. 4a.

We encode three different pairs of images with these resonator pixels. Figures 4b-d show electron microscopy images of three different metasurfaces with encoded images.



$D_x(\text{nm})$	820	560	220	610
$D_y(\text{nm})$	600	670	220	510
Forw.	Dark	Bright	Dark	Bright
Backw.	Bright	Dark	Dark	Bright



**Figure 4. Asymmetric parametric generation of images with nonlinear metasurfaces.** (a) Set of four meta-atoms ( $\alpha$ - $\delta$ ) on a glass substrate in air. All the meta-atoms consist of silicon (grey) layer 480 nm thick and silicon nitride layer (green) 360 nm thick. The meta-atoms are arranged into a square lattice with 900 nm period. Elliptical geometries of the meta-atoms in XY plane are described in the bottom part of (a). The  $\alpha$ - $\delta$  meta-atoms produce four different combinations of responses for forward and backward illumination as specified in the bottom part of (a). (b-d) Electron microscope images of three different metasurfaces layouts assembled from the set of four meta-atoms. (e-g) their nonlinear optical response detected in transmission at third harmonic frequency to forward and backward excitation at 1475 nm wavelength.

The metasurface featured in Fig. 4b presents the simplest case as it consists of only two types of nanoresonators ( $\alpha$  &  $\beta$ ). Figure 4e on its left side shows a pair of black and white images encoded into this metasurface – one image for “forward” and one image for “backward” excitation correspondingly. In “forward” direction, the metasurface generates a bright square, and in “backward” direction, it features a bright circle with embedded dark square. The right side of Fig. 4e shows experimentally observed distributions of third harmonic signal across the metasurface as seen in the transmission direction. Experimental observations match closely theoretical design.

We next proceed with metasurfaces consisting of all four types of nanoresonator pixels that can generate completely independent images for “forward” and “backward” scenarios. Figures 4c,f feature a metasurface producing a simple independent pair of images: an image of stripes (forward) and a chess-board pattern (backward). Figures 4d,g features a metasurface with encoded pair of arbitrarily images: a contour of Australia and a stylistic image of a Sydney Opera House. Experimentally observed field distributions resemble closely encoded images.

In conclusion, we have designed and demonstrated metasurfaces with flexible control over the nonlinear light generation. The metasurfaces consist of all-dielectric nanoresonators supporting both electric and magnetic Mie resonances. Asymmetry of the nanoresonators’ design leads to magneto-electric coupling within the resonators. In the regime of linear light-matter interactions, the coupling results in different multipolar composition of nanoresonators’ scattering, while keeping the total scattering unchanged. The coupling leads to a drastic suppression of a magnetic dipole resonance for one direction of excitation, and a substantial enhancement of the magnetic dipole for the reversed direction of excitation. Once nonlinear optical effects are added, the suppression/enhancement of the magnetic dipole mode leads to suppression/enhancement of nonlinear third harmonic generation. We demonstrate flexibility of engineering of asymmetric harmonic generation by demonstrating metasurfaces that generate different images at the third harmonic wavelength when illuminated from the opposite sides. These nonuniform metasurfaces are assembled from a set of dissimilar nanoresonators with varying types of asymmetries in their nonlinear responses.

The ability to engineer optical interactions beyond the electric dipole modes with a strong optically induced magnetic response and effective magneto-electric coupling pave the way towards novel functionalities of nonlinear nanoscale optical metadevices beyond the limitation of linear optics. We envision the development of subwavelength resonators and metasurfaces governed by the interplay between magneto-electric coupling and nonlinear light-matter interactions. Functionalities of such resonators can go beyond parametric generation of light, and the principles laid in this work may find applications in asymmetric generation of entangled photon states as well as in asymmetric self-action effects leading to nonreciprocity and optical isolation at a level of individual nanoresonators.

## METHODS

**Numerical calculations.** We simulate the generation of the third harmonic signal using the finite-element-method solver in COMSOL multiphysics in the frequency domain. All our simulations consider a single nanoresonator in a unit cell with periodic boundary conditions, that is the simulations consider the coupling between identical neighbouring nanoresonators, but do not account for differences in coupling between non-identical nanoresonators. Our nonlinear calculations are based on undepleted pump approximation and are performed in two stages. Upon the first stage, we calculate linear light-matter interactions, retrieve optical field distributions at the fundamental frequency in the nanoresonator. We then deduce the nonlinear polarization component from linear field distributions. At the second stage, we employ this as a source of the third harmonic generation. We approximate the  $\chi^{(3)}$  tensor for amorphous silicon to a non-dispersive scalar value of  $2.45 \times 10^{-19} \text{ m}^2/\text{V}^2$ .

To find an optimal design for the nanoresonators, we optimize the parameter space of five geometrical dimensions: thickness of each material layer ( $h_1, h_2$ ), long and short axes of ellipses ( $D_1, D_2$ ), and the square unit cell size ( $P$ ) (this is reduced to four parameter space for the homogeneous metasurface).

To enhance the computing speed, we implement the multigoal global genetic optimization algorithms to guide the COMSOL calculations. This method analyses the calculated data sets in each generation as goal functions with the corresponding selecting criteria depending on the desirable characteristics: E.g., selecting criteria for metasurface are (s1) & (s2). For atom type  $\delta$  in Fig4 are (s1) & (s3). Other atom types et cetera. (s1) Third harmonic conversion efficiency in the desirable illumination direction. (s2) Third harmonic intensity contrast between the forward and backward illumination regimes. (s3) THG predominantly in the direction of transmission of the incident wave for both cases of illumination. The geometrical parameters set of the nanoresonators are treated as genomes in this algorithm that evolve to reach optimization.

**Nanofabrication.** The metasurfaces were fabricated on a glass substrate using a multi-step process that begins with consecutive deposition of thin films of amorphous silicon (a-Si) and silicon nitride ( $\text{SiN}_x$ ) of desired thicknesses by plasma-enhanced chemical vapor deposition (PECVD). For the homogeneous metasurface (Fig. 3), a silicon nitride thin film was deposited first followed by the deposition of an amorphous silicon film, while for the inhomogeneous metasurface (Fig. 4), the silicon nitride film was deposited after the amorphous silicon film. A poly-methyl-methacrylate (PMMA) resist layer was spin-coated onto the bilayer films and baked on a hot plate at  $170^\circ\text{C}$  for 2 min to remove the solvent. Then, the desired patterns were transferred by using a standard electron beam lithography and subsequent development in 1:3 methyl isobutyl ketone (MIBK): isopropyl alcohol (IPA) solution. Next, a 20 nm thick Chromium (Cr) mask was deposited by electron beam evaporation. After a lift-off process in hot acetone, the patterns were transferred from PMMA to Cr. Finally, the structures were transferred onto the bilayer material using an inductively coupled plasma reactive ion etching (ICP-RIE) and the subsequent removal of the Cr mask by a commercially purchased Cr-etch solution. Note, each material-layer within the bilayer film was etched by a recipe optimised to that specific material. Electron microscope images of the resulting sample were obtained using a scanning electron microscope. The homogeneous metasurfaces was further embedded into a droplet of optical oil with refractive index like that of the glass substrate and covered by a glass slide identical to the substrate slide.

**Optical measurements.** For linear spectral measurements, a tungsten halogen light bulb was used as a light source. For nonlinear optical measurements, a pulsed laser system was used in the experiments as a light source. It consisted of Femtolux Ekspla laser (1030 nm wavelength) and Hotlight Systems MIROPA optical parametric amplifier (1350-1750 nm wavelengths tunability range). Optical pulses with 6ps duration, 5MHz repetition rate, linear horizontal polarization was used. The average output power of the laser system was 500mW at 1450 nm wavelength decreasing for other wavelengths. The power was monitored by an Ophir IR power meter. The collimated laser beam was narrowed down by achromatic doublet lenses from Thorlabs to illuminate an area twice as large as an individual metasurface. Both the infrared (IR) excitation and the visible

(VIS) generated third-harmonic signal was captured by an objective lens Mitutoyo Plan Apo NIR HR X100 NA0.7 with an achromatic performance across 400-1800 nm spectral range. The IR spectra were measured with a spectrometer NIR-Quest by Ocean Optics, and VIS spectra were monitored by a spectrometer QE Pro by Ocean Optics. The metasurface images in the IR were recorded on a camera Xenics Bobcat 320 paired with an infinity-corrected  $f=150$  mm IR achromatic doublet lens from Thorlabs. The metasurface images in the VIS were recorded on a camera Trius-SX694 Starlight Xpress paired with an infinity-corrected  $f=150$  mm VIS achromatic doublet lens from Thorlabs. For measurements at the third-harmonic frequency, the excitation wavelength was filtered by a colour glass FGB900. “Forward” and “Backward” illumination directions were recorded by flipping the sample around the vertical axis. Experimental “Backward” images were correspondingly mirrored along the vertical axis in post-processing. An aperture diaphragm was added in the back focal plane of the imaging objective ensuring the collection of only forward-propagating signal. The resolution of “forward” images is reduced in comparison to “backward” images by aberrations introduced by the substrate.

## **ACKNOWLEDGEMENTS**

The authors thank V. Asadchy, A. Alu, C. Caloz, A. Poddubny, D. Smirnova, K. Simovski, I. Shadrivov, and S. Tretyakov for numerous stimulating discussions. The authors acknowledge the use of the nanofabrication facility at the Paderborn University and acknowledge the Australian National Fabrication Facility, ACT Node, for access to the SEM facilities. S.K. acknowledges a support from the Alexander von Humboldt Foundation and the Australian Research Council (DE210100679). Z.D. acknowledges help from F. Tjiptoharsono with the fabrication etching recipe. T.Z. acknowledges funding by the European Research Council (ERC) under the European Union's Horizon 2020 research and innovation program (grant agreement No. 724306). L.W. acknowledges supports from Jiangsu NSF project (BK20200393), National Key R&D Program of China (2020YFB1806603), Scientific Research Start-up Project of New Faculties of Southeast University. Y.K. acknowledges a support from the Strategic Fund of the Australian National University, the Australian Research Council (grant DP210101292), and the US Army International Office (grant FA520921P0034).

## REFERENCES

1. S. S. Kruk and Y. S. Kivshar, "Functional Meta-Optics and Nanophotonics Govern by Mie Resonances," *ACS Photonics* **4**, 2638–2649 (2017).
2. W. T. Chen, A. Y. Zhu, and F. Capasso, "Flat optics with dispersion-engineered metasurfaces," *Nat. Rev. Mater.* **5**, 604–620 (2020).
3. S. M. Kamali, E. Arbabi, A. Arbabi, and A. Faraon, "A review of dielectric optical metasurfaces for wavefront control," *Nanophotonics* **7**, 1041–1068 (2018).
4. G. Li, S. Zhang, and T. Zentgraf, "Nonlinear photonic metasurfaces," *Nat. Rev. Mater.* **2**, 17010 (2017).
5. A. Krasnok, M. Tymchenko, and A. Alù, "Nonlinear metasurfaces: a paradigm shift in nonlinear optics," *Mater. Today* (2017).
6. V. Zubyuk, L. Carletti, M. Shcherbakov, and S. Kruk, "Resonant dielectric metasurfaces in strong optical fields," *APL Mater.* **9**, 060701 (2021).
7. M. R. Shcherbakov, D. N. Neshev, B. Hopkins, A. S. Shorokhov, I. Staude, E. V. Melik-Gaykazyan, M. Decker, A. A. Ezhov, A. E. Miroshnichenko, I. Brener, A. A. Fedyanin, and Y. S. Kivshar, "Enhanced Third-Harmonic Generation in Silicon Nanoparticles Driven by Magnetic Response," *Nano Lett.* **14**, 6488–6492 (2014).
8. V. F. Gili, L. Carletti, A. Locatelli, D. Rocco, M. Finazzi, L. Ghirardini, I. Favero, C. Gomez, A. Lemaître, M. Celebrano, C. De Angelis, and G. Leo, "Monolithic AlGaAs second-harmonic nanoantennas," *Opt. Express* **24**, 15965 (2016).
9. R. Camacho-Morales, M. Rahmani, S. Kruk, L. Wang, L. Xu, D. A. Smirnova, A. S. Solntsev, A. Miroshnichenko, H. H. Tan, F. Karouta, S. Naureen, K. Vora, L. Carletti, C. De Angelis, C. Jagadish, Y. S. Kivshar, and D. N. Neshev, "Nonlinear Generation of Vector Beams from AlGaAs Nanoantennas," *Nano Lett.* (2016).
10. S. Liu, M. B. Sinclair, S. Saravi, G. A. Keeler, Y. Yang, J. Reno, G. M. Peake, F. Setzpfandt, I. Staude, T. Pertsch, and I. Brener, "Resonantly Enhanced Second-Harmonic Generation Using III–V Semiconductor All-Dielectric Metasurfaces," *Nano Lett.* **16**, 5426–5432 (2016).
11. G. Grinblat, Y. Li, M. P. Nielsen, R. F. Oulton, and S. A. Maier, "Enhanced Third Harmonic Generation in Single Germanium Nanodisks Excited at the Anapole Mode," *Nano Lett.* **16**, 4635–4640 (2016).
12. Y. Yang, W. Wang, A. Boulesbaa, I. I. Kravchenko, D. P. Briggs, A. Puretzky, D. Geohegan, and J. Valentine, "Nonlinear Fano-Resonant Dielectric Metasurfaces," *Nano Lett.* **15**, 7388–7393 (2015).
13. K. Koshelev, S. Kruk, E. Melik-Gaykazyan, J.-H. Choi, A. Bogdanov, H.-G. Park, and Y. Kivshar, "Subwavelength dielectric resonators for nonlinear nanophotonics.," *Science* **367**, 288–292 (2020).
14. T. Schlickriede, C.; Waterman, N.; Reineke, B.; Georgi, G.; Zhang, S.; Zentgraf, "Imaging through nonlinear metalens using second harmonic generation," *Adv. Opt. Mater.* 1703843 (2018).
15. C. Schlickriede, S. S. Kruk, S. S. Kruk, L. Wang, B. Sain, Y. Kivshar, and T. Zentgraf, "Nonlinear Imaging with All-Dielectric Metasurfaces," *Nano Lett.* **20**, 4370–4376 (2020).
16. G. D'Aguanno, Y. Hadad, D. A. Smirnova, X. Ni, A. B. Khanikaev, and A. Alù, "Nonlinear topological transitions over a metasurface," *Phys. Rev. B* **100**, 214310 (2019).
17. Z. Huang, A. Baron, S. Larouche, C. Argyropoulos, and D. R. Smith, "Optical bistability with film-coupled metasurfaces," *Opt. Lett.* **40**, 5638 (2015).
18. S. Divitt, W. Zhu, C. Zhang, H. J. Lezec, and A. Agrawal, "Ultrafast optical pulse shaping using dielectric metasurfaces," *Science* (80-. ). **364**, 890–894 (2019).
19. K. Gallo, G. Assanto, K. R. Parameswaran, and M. M. Fejer, "All-optical diode in a periodically poled lithium niobate waveguide," *Appl. Phys. Lett.* **79**, 314–316 (2001).
20. S. Lepri and G. Casati, "Asymmetric Wave Propagation in Nonlinear Systems," (n.d.).
21. F. Biancalana, "All-optical diode action with quasiperiodic photonic crystals," *J. Appl. Phys.* **104**, 93113 (2008).
22. N. Bender, S. Factor, J. D. Bodyfelt, H. Ramezani, D. N. Christodoulides, F. M. Ellis, and T. Kottos, "Observation of Asymmetric Transport in Structures with Active Nonlinearities," (2013).
23. E. Poutrina and A. Urbas, "Multipolar interference for non-reciprocal nonlinear generation," *Sci. Rep.* **6**, 25113 (2016).
24. K. H. Kim, "Asymmetric Second-Harmonic Generation with High Efficiency from a Non-chiral Hybrid Bilayer Complementary Metasurface," *Plasmonics* 1–6 (2020).

25. M. Lawrence, D. R. Barton, and J. A. Dionne, "Nonreciprocal Flat Optics with Silicon Metasurfaces," *Nano Lett.* **18**, 1104–1109 (2018).
26. B. Jin and C. Argyropoulos, "Self-Induced Passive Nonreciprocal Transmission by Nonlinear Bifacial Dielectric Metasurfaces," *Phys. Rev. Appl.* **13**, 054056 (2020).
27. L. Cheng, R. Alaei, A. Safari, M. Karimi, L. Zhang, and R. W. Boyd, *Superscattering, Superabsorption, and Nonreciprocity in Nonlinear Antennas* (2020).
28. N. Shitrit, J. Kim, D. S. Barth, H. Ramezani, Y. Wang, and X. Zhang, "Asymmetric Free-Space Light Transport at Nonlinear Metasurfaces," *Phys. Rev. Lett.* **121**, 046101 (2018).
29. V. S. Asadchy, A. Díaz-Rubio, and S. A. Tretyakov, "Bianisotropic metasurfaces: Physics and applications," *Nanophotonics* **7**, 1069–1094 (2018).
30. Y. Zhao, M. A. Belkin, and A. Alù, "Twisted optical metamaterials for planarized ultrathin broadband circular polarizers," *Nat. Commun.* **3**, 1–7 (2012).
31. Y. Svirko, N. Zheludev, and M. Osipov, "Layered chiral metallic microstructures with inductive coupling," *Appl. Phys. Lett.* **78**, 498–500 (2001).
32. C. Menzel, C. Helgert, C. Rockstuhl, E. B. Kley, A. Tünnermann, T. Pertsch, and F. Lederer, "Asymmetric transmission of linearly polarized light at optical metamaterials," *Phys. Rev. Lett.* **104**, 253902 (2010).
33. C. Pfeiffer, C. Zhang, V. Ray, L. J. Guo, and A. Grbic, "High performance bianisotropic metasurfaces: Asymmetric transmission of light," *Phys. Rev. Lett.* **113**, 023902 (2014).
34. Y. Ra'Di, V. S. Asadchy, and S. A. Tretyakov, "Tailoring reflections from thin composite metamirrors," *IEEE Trans. Antennas Propag.* **62**, 3749–3760 (2014).
35. M. Albooyeh, R. Alaei, C. Rockstuhl, and C. Simovski, "Revisiting substrate-induced bianisotropy in metasurfaces," *Phys. Rev. B - Condens. Matter Mater. Phys.* **91**, 195304 (2015).
36. D. V. Zhirihin, S. V. Li, D. Y. Sokolov, A. P. Slobzhanyuk, M. A. Gorlach, and A. B. Khanikaev, "Photonic spin Hall effect mediated by bianisotropy," *arXiv* **44**, 1694–1697 (2018).
37. A. A. Gorlach, D. V. Zhirihin, A. P. Slobzhanyuk, A. B. Khanikaev, and M. A. Gorlach, "Photonic Jackiw-Rebbi states in all-dielectric structures controlled by bianisotropy," *Phys. Rev. B* **99**, 205122 (2019).
38. A. Slobzhanyuk, S. H. Mousavi, X. Ni, D. Smirnova, Y. S. Kivshar, and A. B. Khanikaev, "Three-dimensional all-dielectric photonic topological insulator," *Nat. Photonics* **11**, 130–136 (2016).
39. M. Kerker, D.-S. Wang, and C. L. Giles, "Electromagnetic scattering by magnetic spheres," *J. Opt. Soc. Am.* **73**, 765 (1983).
40. M. Decker, I. Staude, M. Falkner, J. Dominguez, D. N. Neshev, I. Brener, T. Pertsch, and Y. S. Kivshar, "High-Efficiency Dielectric Huygens' Surfaces," *Adv. Opt. Mater.* **3**, 813–820 (2015).
41. M. Albooyeh, V. S. Asadchy, R. Alaei, S. M. Hashemi, M. Yazdi, M. S. Mirmoosa, C. Rockstuhl, C. Simovski, and S. A. Tretyakov, "Purely bianisotropic scatterers," *Phys. Rev. B* **94**, 245428 (2016).
42. Y. Ra'Di and S. A. Tretyakov, "Balanced and optimal bianisotropic particles: Maximizing power extracted from electromagnetic fields," *New J. Phys.* **15**, 053008 (2013).